Functional Role and Prognostic Significance of CD157 in Ovarian Carcinoma

UNIVERSITÀ DEGLI STUDI DI TORINO

Functional role and prognostic significance of CD157 in ovarian carcinoma.

Erika Ortolan, Riccardo Arisio, Simona Morone, Paola Bovino, Nicola Lo-Buono, Giulia Nacci, Rossella Parrotta, Dionyssios Katsaros, Ida Rapa, Giuseppe Migliaretti, Enza Ferrero, Marco Volante, Ada Funaro.

Affiliations of authors: Department of Genetics, Biology and Biochemistry University of Turin Medical School, Turin, Italy (EO, SM, PB, NLB, GN, RP, EF, AF), Research Center on Experimental Medicine (CeRMS) University of Turin Medical School, Turin, Italy (EO, EF, AF); Department of Pathology, Sant'Anna Hospital, Turin, Italy (RA); Department of Obstetrics and Gynecology, Gynecologic Oncology and Breast Cancer Unit, University of Turin, Turin, Italy (DK); Department of Public Health and Microbiology, University of Turin, Turin, Italy (GM); Department of Clinical and Biological Sciences, San Luigi Hospital, University of Turin, Turin, Italy (IR, MV).

Address correspondence to:
Ada Funaro, PhD
Laboratory of Immunogenetics
Department of Genetics, Biology and Biochemistry
University of Turin Medical School
Via Santena 19
10126 TURIN, Italy
phone: 0039 011 6705991
fax: 0039 011 6966155
e.mail: ada.funaro@unito.it

Abstract

Background. CD157, a cell surface molecule belonging to the ADP-ribosyl cyclase family, regulates leukocyte diapedesis during inflammation. The parallels between diapedesis and tumor migration, and evidence of CD157 expression in mesothelial cells, led us to investigate the role of CD157 in ovarian carcinoma (OvCa).

Methods. Surgically obtained OvCa and mesothelial cells, and native and engineered OvCa cell lines were assayed for CD157 expression, adhesion to extracellular matrices, migration and invasion. Dissemination and invasion of mesothelium by serous OvCa was investigated using a 3D culture model. Experiments were performed with or without CD157 blocking antibodies. CD157 expression was examined by immunohistochemistry in tissue sections from OvCa patients and compared with clinical parameters. CD157 expression was quantified as H-score and categorized as at/above or below the median value (= 60). Statistical tests were two-sided.

Results. CD157 was expressed by OvCa and mesothelium and it controlled adhesion, migration and invasion of serous OvCa through different extracellular matrices. CD157-transfected OvCa cells migrated twice as much as $CD157^-$ control (P = .001). Blockage of CD157 inhibited mesothelial invasion of serous OvCa in a 3D model. The results inferred in vitro were validated by clinical evidence. CD157 was expressed by 93% of epithelial OvCa (n = 82). In serous OvCa, patients with CD157 H-score ≥60 had a significantly shorter DFS and OS than patient with CD157 H-score <60 (CD157 H-score ≥60: median DFS = 18 months, 95% CI = 5.92 to 30.07 *vs.* CD157 H-score <60: median DFS = unreached ; log-rank test, P = .005; CD157 H-score ≥60: median OS = 45 months, 95% CI = 21.21 to 68.79 *vs.* CD157 H-score <60: median OS = unreached; log-rank test, P = .024). Multivariable Cox regression showed that CD157 is an independent prognostic factor for recurrence (HR = 3.008, 95% CI = 1.351 to 6.694; P = .007) and survival (HR = 3.443, 95% CI = 1.273 to 9.308, P = .015).

Conclusions. CD157 plays a pivotal role in the control of OvCa migration and peritoneal invasion, and may be clinically useful as a prognostic tool and therapeutic target.

Introduction

Ovarian carcinoma is among the most lethal of gynecological malignancies and has an extremely poor prognosis (1). This is primarily due to the inability to detect the tumor at an early stage (2), consequently, most patients are diagnosed at an advanced stage of disease when the tumor has spread throughout the peritoneum.

The majority of OvCa arise from the surface epithelium which overlies the ovary and lines postovulatory inclusion cysts (3). OvCa may spread by direct extension to adjacent organs, and malignant cells may exfoliate and be transported by normal peritoneal fluid as multi-cellular aggregates or spheroids (4). Discrete steps of the implant of the tumor are its adhesion to mesothelial cells, migration throughout and invasion of the omentum and peritoneum (5, 6). Seeding into the peritoneal cavity is frequently associated with ascites formation. Dissemination of OvCa through the vasculature is generally rare, although the presence of metastases in extra-peritoneal sites (e.g., bone marrow, brain and liver) has been described in advanced-stage disease (7, 8).

The mesothelium, a single layer of cells covering the peritoneal cavity and its organs, is the first barrier encountered by OvCa cells and the major site of tumor dissemination. Mesothelial cells release different inflammatory mediators, ECM proteins, adhesion molecules and chemotactic factors that foster peritoneal metastases (9, 10). The development of peritoneal metastases is regulated by a set of interacting molecules expressed by the tumor and/or mesothelium and occurs in sequential steps (5, 11). The molecular mechanisms that control invasion into the surrounding stroma and dissemination to the peritoneum are still unidentified.

It is known that dissemination of tumor cells shares several steps with leukocyte extravasation, a physiological process in which ectoenzymes play important roles (12). One of these ectoenzymes is CD157, a glycosylphosphatidylinositol (GPI)-anchored glycoprotein encoded by a member of the NADase/adenosine diphosphate (ADP)-ribosyl cyclase gene family which also encodes CD38 (13, 14). Although initially characterized as a stromal (15) and myeloid surface

antigen (16), CD157 is also expressed by other selected cell types (17), including vascular endothelial cells (18) and mesothelial cells (19). It is involved in a number of cellular functions (20-22) and participates in signal transduction through interactions with transmembrane partner molecules (23,24). Evidence indicates that CD157 is a key molecule in the control of leukocyte adhesion and migration, acting both on leukocytes and endothelial cells (18,25).

The expression of CD157 by mesothelial cells (19), which share biological properties and embryonic origin with ovarian surface epithelial cells, led us to hypothesize that it might be also expressed by epithelial OvCa cells and involved in interactions between the mesothelium and tumor cells, ultimately controlling OvCa dissemination.

The results obtained confirmed the working hypothesis, indicating that CD157 i) is expressed by epithelial OvCa, both in tissues and primary cell cultures and cell lines, as well as by primary peritoneal mesothelial cells. Furthermore, it ii) controls OvCa cell migration and invasion on matrigel, fibronectin, laminin and collagen and, iii) regulates peritoneal dissemination and mesothelial invasion of serous epithelial OvCa cells in vitro. The results obtained in vitro are confirmed in vivo, where iv) CD157 is a prognostic factor for tumor recurrence in OvCa and a powerful predictive variable for disease recurrence and survival in the serous histotype.

Methods

Antibodies and reagents.

The anti-CD157 (SY/11B5, IgG1) (26), anti-β1 integrin/CD29 (Moon-4, IgG1) monoclonal antibodies (mAb) and irrelevant murine monoclonal IgG (mIgG) (produced in-house) were affinity purified on protein G (Sigma-Aldrich). RF3 (anti-CD157, IgG2a) mAb was from MBL International (Milan, Italy). Affinity purified, $F(ab')_2$ fraction of goat antibodies to mouse IgG labeled with FITC [$F(ab')_2$-GαMIgG-FITC] was from Jackson ImmunoResearch (LiStarfish, Milan, Italy). $F(ab')_2$ fraction of goat antibodies to mouse IgG labeled with Alexa-488 [Alexa Fluor®-488-$F(ab')_2$-GαMIgG] was from Molecular Probe (Milan, Italy). Fibronectin (FN), Collagen type I (Coll I), and crystal violet were from Sigma-Aldrich (Milan, Italy) and laminin (LN) from BD Biosciences (Milan, Italy).

Cell culture and transfection procedure.

The human OvCa cell lines SKOV-3, NIH:OVCAR-3, NIH:OVCAR-5 were purchased from American Type Culture Collection. The A2780, IGROV-1 and OV-90 lines were kindly provided by M.F. Di Renzo (Institute for Cancer Research and Treatment, Candiolo, Italy) and OC314, OC315 and OC316 lines by S. Ferrini, (Institute for Cancer Research, Genoa, Italy). Cells were grown in the recommended medium and conditions.

NIH:OVCAR-3 cells were transfected with the eukaryotic expression vector pcDNA3.1 (Invitrogen, San Giuliano Milanese, Italy) containing either full-length cDNA for *CD157* or no insert (mock) by using Lipofectamine (Invitrogen). Stable clones were selected in medium containing (200 μg/ml) G418 (Sigma-Aldrich).

Isolation and culture of primary ovarian cancer and mesothelial cells.

OvCa cells were obtained from tumor biopsies and/or neoplastic ascites from patients undergoing surgery and/or paracentesis (collected at the Department of Pathology of the Sant'Anna Gynacological Hospital, Turin, Italy). Written informed consent was obtained from patients enrolled in the study.

Primary cultures were established from tumor fragments dissociated either mechanically or enzymatically and cell suspension filtered to remove clamps. Ascites were centrifuged and cell pellets treated with erythrocyte lysis buffer. OvCa cells were grown in MCDB105/M199 (1:1 ratio, Sigma-Aldrich) supplemented with 20% fetal calf serum (FCS) and experiments were performed at passages 3-8. Cell purification was verified by positive staining for CA-125 (data not shown).

Three primary human peritoneal mesothelial cell (HPMC) cultures were used for the present study. HPMC 2293 was derived from the peritoneal washing of a patient with a mature ovarian teratoma, HPMC 3361 and HPMC 7916 from the peritoneal washing of patients with endometrioid cystadenoma of the ovary. All samples were free of tumor cells, as determined by cytological analysis of cytospin preparations, and contained high percentages of mesothelial cells. HPMC were isolated as described in (5). The mesothelial origin of the cells was verified by vimentin, cytokeratin 8 and calretinin positivity and CD31 negativity (data not shown). HPMC at early passages (1-4) were used for the experiments to minimize dedifferentiation and modifications of the original phenotype.

Reverse transcription-PCR analysis.

Total RNA was purified from ~1 x 10^6 cells using the TRI Reagent (Sigma-Aldrich), and cDNA transcribed from total RNA (2-5 μg) using SuperScript II RT (Invitrogen), according to the manufacturer's instructions. The primers used were as follows: CD157, 5'-GAGATATCCGAGCGAGAG-3' (sense) and 5'-GGACATCGTTTTCCCAG-3'(antisense); β-actin, 5'-CCAAGGCCAAACCGCGAGAAGATGAC-3' (sense) and 5'-AGGGTACATGGTGGTGCCGCCAGAC-3'(antisense).

The PCR reaction conditions for CD157 were: 49 cycles of 30 seconds denaturation at 95 °C, 1 minute (min) annealing at 55 °C, 90 seconds extension at 72 °C. The PCR reaction conditions for β-actin housekeeping gene were: 30 cycles of 1 min denaturation at 94 °C and 2 min annealing at

72 °C. PCR products were analyzed on 1% agarose gel stained with ethidium bromide (Sigma-Aldrich).

Immunoprecipitation and Western Blot Analysis.

Immunoprecipitation was performed as described (24), the precipitated molecule was resolved by sodium dodecyl sulphate-polyacrylamide gel electrophoresis (10%) under reducing conditions and transferred to a PVDF membrane. The membrane was blocked and probed with anti-CD157 mAb, followed by horseradish peroxidase-conjugated secondary antibody (Bio-Rad, Milan, Italy). The immunoreactive bands were visualized by ECL (Perkin Elmer, Monza, Italy).

Immunofluorescence staining.

Cells were incubated with the indicated mAb (5 μg/ml) for 30 min at 4 °C followed by $F(ab')_2$-GαMIg-FITC for 30 min at 4 °C. Fluorescence was analyzed using a FACSCalibur flow cytometer using CellQuest software (BD Biosciences). Background mAb binding was estimated by means of isotype-matched irrelevant control mAb. Ten thousand events were considered for each analysis. Three independent readings were obtained from separate experiments.

Cells for confocal microscopy experiments were grown on gelatin-coated coverslips or in chamber slides (Nunc International, Euroclone, Milan, Italy), fixed with 2% paraformaldehyde (PFA), incubated in PBS containing 20% FCS for 30 min at 20 °C, and stained with anti-CD157 followed by Alexa Fluor®-488-$F(ab')_2$-GαMIgG (Molecular Probe). The samples were analyzed with an Olympus FV300 laser scanning confocal microscope (Olympus Biosystems, Hamburg, Germany). Cells were imaged using a x60 oil immersion objective (1.4 NA).

Invasion assay.

Cell invasion was measured using a two-chamber Transwell system (8 μm pores; BD Biosciences). The top side of the filter was coated with selected matrices (100 μl), or left uncoated for migration assays. Matrigel phenol red-free preparation (BD Biosciences) diluted in ice-cold medium, was added to transwells (30 $\mu g/cm^2$). In invasion assays through selected ECM, transwells were coated with 10 μg/ml of FN, and Coll I or LN (5 $\mu g/cm^2$). Matrix solutions were

polymerized at 37 °C for 1 hour (h) and equilibrated in serum-free medium. OvCa cells were suspended (10^5 cells/well) in medium with 1% FCS, treated with the indicated mAb (10 μg/ml) for 20 min, and then seeded on the coated filters. Medium containing 10% FCS was added to the lower chamber as the chemoattractant. After 16 h incubation at 37 °C, non-invading cells in the upper chamber were removed with a cotton swab and the filters were fixed with methanol and stained with hematoxylin-eosin. The membranes were mounted and migrated cells were photographed at low magnification (x10). Migrated cells were counted in 8 different medium-power fields for each filter.

Adhesion to ECM proteins assay.

OvCa cells ($4x10^4$/well) pre-treated or not with selected mAb (10 μg/ml) for 20 min were plated in 96-well plates coated with FN, Coll I (both at 10 μg/ml) or LN (5 μg/cm^2). After 1 h at 37 °C, non-adherent cells were removed, adherent cells were fixed with 4% PFA and stained with 0.5% crystal violet for 15 min. After cell lysis with 2% SDS, the absorbance was measured at 595 nm. Each adhesion assay was carried out in quadruplicate and repeated at least twice. Results are expressed as a percentage of adhesion of the mIgG-treated control.

Wound assay.

Wounds were created in confluent OvCa cells using a pipette tip. The cells were then rinsed to remove debris, and medium with 1% FCS was added. Wound healing was observed at 0 and 24 h within the scraped line. Duplicate wells of each condition were examined for each experiment, and experiments were repeated 3 times. Quantitative analysis of the percentage of wound healing was calculated by measuring 20 randomly chosen distances across the wound at time 0 and 24 h, divided by the distance measured at time 0. Images were acquired using the Olympus Biosystems Microscope BX71, equipped with the F-View II camera and the AnalySIS FIVE analysis software (Olympus Biosystems, Hamburg, Germany).

Spheroid formation.

Spheroids were generated using a modification of the hanging droplet method (27). Briefly, cells ($5x10^2$/15 µl of RPMI with 10% FCS) were placed on the cover of a tissue culture dish. The cover was placed over a dish containing 10 ml of PBS to prevent dehydration of the hanging droplets. Spheroid formation was monitored after 4 days.

Spheroid dissemination and mesothelial monolayer invasion assay.

HPMC ($1x10^4$/well) were grown until confluence on 96-well plates. Spheroids (5-10/well) were seeded onto the HPMC monolayer in the constant presence of the indicated mAb (10 µg/ml). Every 24 h, two thirds of the medium was replaced with fresh medium containing the indicated mAb. Spheroids were digitally photographed 1 h after plating (t = 0) and again at 1, 3, and 7 days. Spheroid dissemination was defined as spheroid disaggregation and spreading on top of the HPMC monolayers without forming invasive foci and quantified by calculating the fold change in area (spheroid pixel area at each time point/spheroid pixel area at t = 0). Spheroid invasion was defined as described (28). The percentage of invasion was quantified by counting the invading spheroids: 80-100 spheroids were counted for each experimental condition, from two experiments. Images were acquired using the Olympus Biosystems Microscope BX71, equipped with the F-View II camera and the AnalySIS FIVE software (Olympus Biosystems).

Spheroid disaggregation assay.

The disaggregation assay was performed as previously described (29). Briefly, 96-well plates coated with 10 µg/ml FN and Coll I or 5 µg/cm^2 LN were blocked with BSA (1 mg/ml) for 1 h at 37 °C. Spheroids (5-10 spheroids/well) were seeded on wells in serum-free RPMI 1640 medium. After 30 min at 37 °C, the indicated mAb (10 µg/ml) were added. To track individual spheroids over time, a map of the wells was created. The pixel area of the spheroids at each time points was measured, and the fold change in area was calculated as the ratio between the pixel area of the spheroids at 24 h and at time 0. Results represent the average fold change in area of 50-90 spheroids for each condition.

Adhesion to HPMC assay.

HPMC ($1x10^4$/well) were grown until confluence on 96-well plates and incubated with the indicated mAb (10 μg/ml) for 20 min at 20 °C. OvCa cells treated with the same mAb were added ($4x10^4$/well) to HPMC and allowed to adhere for 1 h at 37 °C in the presence of the mAb. Non adherent OvCa cells were washed off, and the HPMC-OvCa co-cultures were stained with MTT (3-(4,5-dimethylthiazol-2-yl)-2,5-diphenyl tetrazolium bromide) (Sigma-Aldrich) (0.5 mg/ml) for 1 h at 37 °C. DMSO (Sigma-Aldrich) was used to dissolve the formazan crystals and absorbance measured at 570 nm. Tumor cell adhesion was calculated using the formula: ($A_{570/nm}$ of wells containing tumor cells and HPMC)-($A_{570/nm}$ of wells containing HPMC alone). Results were expressed as the percentage of adhesion of the mIgG-treated control.

Patient data.

The study included 88 archival formalin-fixed, paraffin-embedded non-consecutive samples collected between 1996 and 2004 from patients with primary epithelial OvCa surgically treated by the same team at the Sant'Anna Gynecological Hospital, Turin. All of the pathological material, clinical data and follow-up information was obtained from the Department of Pathology at the same hospital. After surgery, 84 patients received a platinum-based adjuvant treatment (14 patients were treated with platinum alone, 60 patients platinum and taxans and 10 with a combination of platinum, taxans and anthracyclines).

The pathological and clinical stage of tumors was assessed according to the 2002 TNM and FIGO staging system and included 30 patients with clinical stages I-II disease and 58 at stages III-IV. The histological type and the grade of tumors were determined by WHO criteria. Follow-up data, including overall survival and disease recurrence, were available for all patients. The median follow-up period calculated from the date of surgery, was 50 months (range, 1-140 months). The Institutional Review Boards approved the use of tissue samples and patients records.

Immunohistochemistry.

CD157 localization was examined on tissue sections (5 μm) from formalin-fixed, paraffin-embedded epithelial OvCa following antigen retrieval in 10 mM citrate buffer (pH 7.5) at 125 °C

for 10 min and at 90 °C for 10 seconds. After treatment with 0.3% H_2O_2 in methanol, sections were incubated with anti-CD157 mAb (RF3) overnight at 4 °C. After washing, CD157 binding was revealed using the EnVision avidin-biotin-free detection kit (Dako S.p.A, Milan, Italy). Slides incubated with dilution buffer alone provided negative controls.

Immunohistochemical reactions were assessed by light microscopy independently by two pathologists, without prior knowledge of the clinical variables, and scored semiquantitatively by using the H-score. For comparison of staining among tissues, the results were quantified by calculation of a complete H-score that considers both staining intensity and the percentage of cells stained at a specific range of intensities. A complete H-score was calculated by summing the products of the percentage of cells stained at a given staining intensity (0-100) and the staining intensity score (0-3) (30). CD157 expression was categorized as at/above (H-score ≥60) or below (H-score <60) the median value (= 60).

Statistical methods and data analysis.

Means, standard deviation, median and range were used to describe the age of patients; other clinicopathological characteristics of OvCa patients were shown in terms of number of cases and grouped according to CD157 H-score (<60 or ≥60). The analysis of the association between CD157 expression in tissue sections and available clinicopathological features was performed using Chi-square test or Fisher's exact test.

Results of invasion, migration, adhesion and disaggregation assays were shown as means and relative 95% Confidence Interval (95%CI). Comparisons among groups were performed with one-way Anova models and the Bonferroni test was used in the post-hoc analysis with the multiple comparison adjustment of the significance level. Spheroid disaggregation assays were plotted as Box and Whisker diagrams and data were analysed using the Kruskal-Wallis nonparametric analysis of variance. Chi-square test was used for the analysis of spheroid invasion.

The disease-free survival (DFS) and overall survival (OS) times (in months) were defined as the time interval from the date of surgery to the date of first recurrence and to the date of death, respectively. The DFS and OS were analysed using the Kaplan-Meier curves, and differences in survival between the groups of patients were assessed using the log-rank test.

Univariate and multivariate survival analysis was performed for all available clinicopathologic variables, including the CD157 H-score, using the Cox proportional hazards regression model. Covariate that were not statistically significantly associated with survival were not removed from the model (complete model). Proportional hazard (PH) assumption was checked using the Grambsh and Therneau correlation with time test and diagnostic plots based on Shoenfeld residuals. Crude and adjusted hazard ratio (HR) with relative 95%CI were shown. Differences were considered statistically significant for two-tailed P values < .05.

Statistical analysis were performed using SPSS Statistics 17 software (Chicago, IL) and R version 2.8 [R Development Core Team (2008). R Foundation for Statistical Computing, Vienna, Austria].

Results

CD157 expression in human epithelial ovarian cancer and peritoneal mesothelial cells. Expression of CD157 was first investigated in fresh samples of ovarian tumors. Surgical specimens of epithelial OvCa were obtained from 6 chemotherapy-naive patients (Table 1) and minced to obtain a single cell suspension. OvCa 622, OvCa 1349, OvCa 1554 and OvCa 2947 expressed CD157 mRNA and membrane protein, while OvCa 860 and OvCa 1996 were negative (Figure 1, A-B).

CD157 expression was also examined in a panel of 9 OvCa lines. SKOV-3, OV-90, OC314 and OC315 expressed CD157 (Figure 1, C-D). In contrast, both mRNA (Figure 1, D) and protein (not shown) were undetectable in OC316, A2780, IGROV-1, NIH:OVCAR-3 and NIH:OVCAR-5 lines. Western blot analysis of CD157 immunoprecipitated from 4 cell lines confirmed that the molecules migrates as a single chain of ~45 kDa (Figure 1, E).

Non-malignant HPMC obtained from 3 peritoneal washings (HPMC 2293, HPMC 3361 and HPMC 7916) were cultured (Figure 1, F) and analyzed for CD157 expression. Cytofluorimetric analysis demonstrated that all HPMC expressed high levels of CD157 (Figure 1, G). Once in culture, confocal microscopy confirmed that confluent HPMC monolayers express CD157, prevalently localized at the intercellular junctions and on the basal surface (Figure 1, H).

CD157 expression in floating and adherent tumor cells.

The next step was the analysis of CD157 during OvCa progression. To this aim, attention was focused on fresh tumor cells present in reactive ascites. Indeed, one third of OvCa patients present with ascites containing exfoliated tumor cells, aggregates or spheroids. Expression of CD157 was compared in mechanically dissociated cells obtained either from the primary tumor or from ascites of a patient with poorly differentiated, papillary serous cystoadenocarcinoma (OvCa 622). Notwithstanding almost all of the cells from the patient's primary tumor were $CD157^+$ (Figure 2, A, left panel), only a limited number of cells freshly isolated from ascites

expressed CD157. After 2-3 days in culture, the same cells as well as spheroids and aggregates re-expressed CD157 (Figure 2, A, right panel), indicating that CD157 expression might be anchorage-dependent. This hypothesis was confirmed by in vitro experiments using OvCa 2947 cells, selected because of their ability to form spheroids. Cells harvested from the primary culture (mostly $CD157^+$) were used to generate spheroids by hanging drop culture. CD157 expression was then evaluated in spheroids in suspension and after 12-24 h in culture. Surface CD157 almost disappeared on floating spheroids, while its expression increased by ~7-fold after 24 h in culture (Figure 2, B). Parallel experiments were analyzed by confocal microscopy. Optically slicing through the floating spheroids indicated that CD157 was expressed almost exclusively on the cells forming the outer layer of the spheroid (Figure 2, C, left panel). Cells released from disaggregated spheroids adhered to the culture plates and became $CD157^+$ (Figure 2, C, middle panel). Two-three days later, the resulting monolayer reacquired a homogeneous expression of CD157, mainly localized at the intercellular junctions (Figure 2, C, right panel).

Role of CD157 in tumor cell interactions with ECM proteins.

The findings obtained indicated that CD157 is involved in the control of serous OvCa cell migration and invasion. Migration of OvCa cells is reported to be driven by adhesion to ECM mediated by integrins (31,32). The submesothelial ECM is characterized by Coll I and FN which abut the mesothelial monolayer, colocalizing with a thin deposit of LN and collagen IV (33). The role of CD157 in tumor progression was investigated by interfering invasion of OvCa cells in matrigel by means of specific mAb. The invasive capacity of cultures obtained from 4 $CD157^+$ primary serous OvCa and 4 OvCa lines was assessed in the presence of a blocking anti-CD157 mAb. Irrelevant mIgG or blocking anti-β1 integrin mAb was used as the control. These experiments demonstrated that i) the invasive potential varies from tumor to tumor, at least in the experimental conditions adopted here; ii) ligation of CD157 caused a significant reduction of invasive activity in all $CD157^+$ primary tumor cells (mean number of migrated

cells/cm^2 in anti-CD157 and mIgG-treated cells: OvCa 622 = 34.17 and 57.10, respectively, difference = 22.93, 95% CI =9.64 to 36.22, *P* = .001; OvCa 1349 = 103.43 and 142.80, respectively, difference = 39.36, 95% CI = 21.61 to 57.12, *P* < .001; OvCa 1554 = 177.68 and 264.68, respectively, difference = 87, 95% CI = 55.16 to 118.84, *P* < .001; OvCa 2947 = 54.01 and 129.90, respectively, difference = 75.88, 95% CI = 56.32 to 95.45, *P* < .001) (Figure 3, A left panel) and cell lines thus far analyzed (mean number of migrated cells/cm^2 in anti-CD157 and mIgG-treated lines: SKOV-3 = 131.23 and 257.36, respectively, difference = 126.13, 95% CI = 77.26 to 175.01, *P* < .001; OV-90 = 74.40 and 114.44, respectively, difference = 40.04, 95% CI = 1.87 to 78.22, *P* = .038; OC314 = 54.68 and 96.06, respectively, difference = 41.38, 95% CI = 21.60 to 61.16, *P* < .001; OC315 = 5.52 and 7.84, respectively, difference = 2.32, 95% CI = 1.12 to 3.52, *P* =.002) (Figure 3, A right panel) but not in CD157-negative lines (Supplementary Figure 1, A). iii) The effects of CD157 binding were independent of the invasive capacity of the tumors. Matrigel invasion by fresh tumor cells and lines was constantly inhibited by ligation of anti-β1 integrin mAb used as the positive control (Figure 3, A).

OvCa 2947 cells, SKOV-3 and OV-90 lines (all CD157$^+$) were selected by virtue of their high invasive potential for testing invasion through more physiological substrates, such as FN, LN and Coll I. Treatment with anti-CD157 mAb led to substantial inhibition of the invasive capacity of OvCa 2947 cells on all the ECM proteins considered (number of anti-CD157 and mIgG-treated cells invading FN = 168.33 and 277.67, respectively, difference = 109.33, 95% CI = 48.09 to 170.58, *P* = .001; invading LN = 214.00 and 383.17, respectively, difference = 169.17, 95% CI = 98.01 to 240.33, *P* < .001; invading Coll I = 141.30 and 319.42, respectively, difference = 178.12, 95% CI = 134.5 to 221.77, *P* < .001) (Figure 3, B, left panel), of SKOV-3 line (number of anti-CD157 and mIgG-treated cells invading FN = 118.83 and 206.4, respectively, difference = 87.57, 95% CI = 42.78 to 132.35, *P* < .001, and invading Coll I = 179.94 and 407.24, respectively, difference = 227.31, 95% CI = 154.91 to 299.70, *P* < .001) (Figure 3, B, middle panel), and of OV-90 line (number of anti-CD157 and mIgG-treated cells

invading FN = 167.16 and 250.74, respectively, difference = 83.58, 95% CI = 7.63 to 159.54, *P* = .030; invading LN = 287.75 and 501.50, respectively, difference = 213.56, 95% CI = 98.93 to 328.19, *P* = .001; invading Coll I = 447.10 and 1082.89, respectively, difference = 635.79, 95% CI = 343.22 to 928.36, *P* < .001) (Figure 3, B, right panel). Treatment of the CD157-negative IGROV-1 line with anti-CD157 mAb did not interfere with its invasive capacity (Supplementary Figure 1, B).

CD157 mediates leukocyte adhesion to ECM proteins by establishing functional and structural links to integrins (24,25). Hence, we wonder whether CD157 influences the attachment of OvCa 2947 tumor cells, SKOV-3 and OV-90 lines to selected ECM proteins. The results obtained indicated that adhesion of serous OvCa cells to FN, LN and Coll I is significantly reduced by mAb ligation of CD157. The inhibition observed was lower than that obtained by blocking β1 integrin either in fresh tumors or tumor lines (Figure 3, C).

CD157 and cell migration.

The relevance of CD157 in tumor migration was assessed by transfecting full-length *CD157* in the poorly invasive, $CD157^-$ NIH:OVCAR-3 line. Two clones showing a homogeneous expression of CD157 [NIH:OVCAR-3-3D11 and NIH:OVCAR-3-2G5 (Figure 4, A)] were used in a scratch-wound motility assay (Figure 4, B). Quantitative analysis showed that NIH:OVCAR-3 expressing CD157 migrated twice as much as the $CD157^-$ control (NIH:OVCAR-3-3D11 mean of migration capacity = 2.17-fold than mock, 95% CI = 1.46% to 2.88%, *P* = .002; NIH:OVCAR-3-2G5 mean of migration capacity = 2.45-fold than mock, 95% CI = 2.32% to 2.58%, *P* = .001) (Figure 4, C).

Role of CD157 in peritoneal dissemination of OvCa cells.

The first step in peritoneal dissemination of OvCa is the adhesion of single cells or cells within spheroids to the mesothelium. Spheroids generated from the OV-90 line were used as an in vitro model to mimic the conditions that tumor cells face in vivo (29,34). The ability of

spheroids to disseminate and invade live primary HPMC monolayers was investigated by measuring their disaggregation in the presence of anti-CD157, anti-β1 integrin and irrelevant mIgG mAb.

OV-90 spheroids were seeded on confluent HPMC 2293 for 7 days. Spheroids initially increased in size, spread, disaggregated and then disseminated on the HPMC monolayer (28) establishing foci of invasion by day 3. Spheroid invasion resulted in the establishment of a monolayer of proliferating OvCa cells that replaced the mesothelial layer. In parallel, HPMC retracted exposing the submesothelial ECM and invading tumor cells appeared within the same plane as the HPMC monolayer. Cells unable to invade, disseminated over the HPMC monolayer and were visible in a different focal plane.

The presence of CD157 mAb did not block enlargement of the spheroids (appreciable by day 3) or the spread and dissemination over the HPMC (Figure 5, A), but did interfere with the invasion of the monolayer (Figure 5, B). By day 7, the disseminating ability of spheroids exposed to anti-CD157 mAb was significantly higher than that of the control [median increase in the area of spheroids = 66.49-fold (IQR = 52.25 to 73.73) in CD157-treated *vs.* 39.44-fold (IQR = 23.06 to 56.41) in IgG-treated spheroids, P = .001] (Figure 5, A): tumor cells proliferated and grew, forming a layer on top of HPMC (Figure 5, B). By days 1 and 3, anti-CD157 mAb, and by day 3 and 7 anti-β1-integrin mAb, are apparently uninfluential on spheroid dissemination. However, definitive conclusions cannot be drawn due to the large variance of experiments.

The disseminating potential of anti-CD157-treated cells was accompanied by a decreased invasive capacity. Actively invading spheroids were counted at days 1, 3 and 7. After 7 days in the presence of anti-CD157 mAb, only ~35% of spheroids were able to break and invade the mesothelial layer. Approximately 80% of spheroids showed clear invasion of the underlying mesothelium in all other conditions (invading spheroids at day 7 in the presence of anti-CD157 mAb = 35.29%, anti-β1 integrin mAb = 80.00% and mIgG = 80.76%) (Figure 5, C). The

reduction of the invasive ability of spheroids induced by CD157 ligation was not due to prevention of initial spheroid attachment, since the mAb treatment did not alter the adhesive ability of the spheroids (data not shown). Furthermore, CD157 did not play an obvious role in the control of tumor cell adhesion to HPMC (Figure 5, D).

As a result of tumor invasion, the basal membrane underlying the mesothelial layer is exposed. The involvement of CD157 in spheroid interactions with the submesothelial basal membrane was assessed by means of a disaggregation assay on various ECM components.

Spheroids were allowed to adhere to ECM-coated wells for 30 min before the addition of anti-CD157, anti-β1 integrin or irrelevant mIgG mAb. On FN and LN, tumor cells migrated outward from mIgG-treated spheroids, resulting ~8-fold and ~6-fold change in area, respectively, over 24 h. Ligation of CD157 reduced the spheroid disaggregation area on FN and LN by >50% compared to the control (mean fold increase in area of anti-CD157 and mIgG-treated spheroids on FN = 4.03 and 8.17, respectively, difference = 4.14, 95% CI = 2.90 to 5.37, $P < .001$; on LN = 3.56 and 6.13, respectively, difference = 2.57, 95% CI = 1.74 to 3.40, $P < .001$) (Figure 5, E-F). The spheroids totally disaggregated on Coll I: cells migrated outward and spread to form a monolayer at the site of initial spheroid attachment, resulting in 15.51-fold (95% CI = 13.33 to 17.68) increase in area. Incubation with anti-CD157 mAb did not significantly interfere with spheroid disaggregation on thin Coll I gel or on dense gel (0.6 mg/ml, data not shown). As expected (29,35), spheroid disaggregation on all the ECM considered was strictly dependent on β1 integrin ($P < .001$, Figure 5, E).

CD157 expression and clinicopathological characteristics of human ovarian cancer.

The results of the present work provide compelling evidence that CD157 plays a significant role in migration and dissemination of serous OvCa. The validity of the findings observed in vitro was assessed in vivo by analyzing the characteristics of a sample of OvCa patients. CD157 expression was analyzed by immunohistochemistry on archival material from 88 patients with epithelial OvCa with a known clinical history and compared with clinical

parameters. The cohort included 34% stage I-II (n = 30) and 66% stage III-IV (n = 58) tumors. The sample included serous papillary (n = 51), endometrioid (n = 12), undifferentiated (n = 12), clear cells (n = 9) and mucinous (n = 4) cases (summarized in Table 2).

CD157 was expressed by 93% (n = 82) of tumor samples at varying levels [6 tumors (7%) were negative] and with discrete localization patterns, namely granular cytoplasmic, dot-like cytoplasmic with perinuclear localization and membranous with apical localization (Figure 6, A-C). On specimens containing normal ovarian surface epithelium, CD157 was mainly localized at the intercellular boundaries and at the basolateral surface of the epithelial cells (Figure 6, D). Quantitative CD157 expression levels (defined as H-score) did not associate with any of the clinicopathological features analyzed (Figure 6, E and Table 2). The univariate analysis of DFS and OS performed on all the OvCa patients demonstrated that CD157 expression levels and clinical outcome are associated. Patients with CD157 H-score ≥60 had a significantly shorter DFS than patients with CD157 H-score <60 (CD157 H-score ≥60: median DFS = 30 months, 95% CI = 20.99 to 39.00 *vs.*CD157 H-score <60: median DFS = unreached; log-rank test: $P = .004$) (Figure 7, A). The association between CD157 expression levels and OS showed a clear trend, but did not reach statistical significance (log-rank test, $P = .059$) (Figure 7, B). The association between patient DFS, OS and CD157 expression levels was analyzed in serous (n = 51) *vs.* non-serous (n = 37) ovarian carcinomas. Kaplan-Meier survival analysis showed that a CD157 H-score ≥60 is associated with a significantly shorter DFS and OS in patients with serous carcinoma, the most common and aggressive histotype (CD157 H-score ≥60: median DFS = 18 months, 95% CI = 5.92 to 30.07 *vs.* CD157 H-score <60: median DFS = unreached; log-rank test, $P = .005$; CD157 H-score ≥60: median OS = 45 months, 95% CI = 21.21 to 68.79 *vs* CD157 H-score <60: median OS = unreached, log-rank test, $P = .024$) (Figure 7, C-D). The association is not significant in non-serous carcinomas (Figure 7, E-F).

A multivariable Cox proportional hazard model was used to test the influence on survival of all the available clinicopathologic variables, including CD157 H-score. This analysis revealed that

in addition to the tumor stage (HR = 3.489, 95% CI = 1.531 to 7.949, *P* = .003) and histological type (non serous *vs* serous; HR = 2.139, 95% CI = 1.128 to 4.055, *P* = .020), CD157 H-score was also an independent prognostic factor for DFS in ovarian carcinoma. Patients with CD157 H-score ≥60 had a statistically significant higher risk of tumor recurrence than patients with CD157 H-score <60 (HR = 2.438, 95% CI = 1.247 to 4.764, *P* = .009) (Table 3, A). Multivariable analysis performed on serous carcinoma confirmed that CD157 is an independent prognostic factor of tumor relapse (HR = 3.008, 95% CI =1.351 to 6.694, *P* = .007) (Table 3, A) and overall survival (HR = 3.443, 95% CI = 1.273 to 9.308; *P* = .015) (Table 3, B).

Discussion

CD157 controls leukocyte diapedesis in inflammatory conditions (18,22), a physiological process similar to that exploited by tumor cells to migrate to secondary sites. We hypothesized that the role of CD157 might extend beyond that of controlling leukocyte trafficking to include more general regulation of cellular invasive and migratory activities, including cancer cell dissemination. The model adopted to test the validity of our hypothesis was dissemination in ovarian carcinoma. The choice was also independently sustained by a recent study showing that BST-1/CD157 is one of the genes differentially expressed by primary cultures of normal ovarian surface epithelia and epithelial OvCa cells (36).

The results of this study provide evidence that CD157 is expressed by epithelial OvCa (both in tissues and primary cell cultures), by cell lines and by peritoneal mesothelial cells. Furthermore, CD157 is involved in the interactions among serous OvCa cells, ECM proteins and mesothelial cells, which ultimately control tumor cell migration and invasion.

The study was extended to OvCa cells and spheroids floating in peritoneal effusions. These are the most typical manifestations of OvCa (particularly serous carcinoma) (1), and are implicated in the metastatic spread of the tumor (37). CD157 expression is down-regulated in cancer cells isolated from ascites as well as in spheroids generated in vitro from $CD157^{+}$ serous primary tumors. Indeed, CD157 expression is restricted to the peripheral cell layer of spheroids, the site of active interaction between the cancer cells and the surrounding microenvironment and the peritoneum, where the metastatic outgrowth occurs. However, when spheroids adhere to the tissue culture plate and give rise to a confluent monolayer, CD157 expression is restored on virtually all of the cells. One possible explanation is that anchorage and/or environmental factors regulate the expression and localization of CD157, much in the same way as with selected integrins (38).

The initial observations suggested that CD157 might be involved in OvCa cell migration and dissemination. To explore this issue, we turned our attention to the role of CD157 in interactions with ECM proteins and mesothelial cells.

The results obtained indicate that CD157 controls adhesion of serous OvCa cells to ECM and their successive invasion. These events are significantly inhibited by blocking anti-CD157 mAb, both in the primary cell cultures obtained from the fresh tumors and in CD157-positive OvCa line models. The inhibitory effects are strictly dependent on the presence of the matrix, while its composition is apparently uninfluential. The incomplete inhibition of adhesion indicates that other molecules participate in this process. Integrins play a leading role in the adhesion of OvCa to ECM (31,39); moreover, they control intracellular signaling pathways that regulate survival, proliferation, gene expression and migration of the tumor cells (40). To accomplish these tasks, integrins must act not only as individual receptors, but also as components of supramolecular complexes on the cell membrane (41). CD157 was recently demonstrated to belong to one of these supramolecular complexes, which includes β2 (24) and β1 integrins (A.F. unpublished observation) on myeloid cells. It is likely that CD157 behaves as a multifunctional protein capable of interacting with integrins (and with other receptors) and modulating multiple biological events, such as adhesion, migration and invasion in different cell types.

A second step of OvCa progression is the implantation of floating aggregates or spheroids on the mesothelium (37), an instrumental step in the development of peritoneal metastases. The mesothelium is compromised by the effects of inflammatory cytokines and soluble factors; as a consequence, the mesothelial cells retract, creating points of access to the underlying ECM through which the tumor cells invade (42). The role of CD157 in controlling this step was analyzed by means of a 3D in vitro model using spheroids generated from the OvCa lines to mimic tumor cell aggregates in peritoneal effusions (43). The interactions between tumor cells and mesothelium are regulated by a network of soluble factors and surface molecules, only

partially identified. The results from this study support the view that CD157 is a key element of this network. In the in vitro system adopted, spheroids adhere to and spread across the top of the HPMC monolayer, giving origin to foci of invasion. The number of foci of tumor cells invading the mesothelial layer is significantly lower when CD157 is blocked. The inhibition is not attributable to mAb-induced anti-proliferative effects, since tumor cells are able to proliferate over the top of the mesothelium, giving rise to dissemination areas that are even larger than in the control spheroids. The inhibitory effects are not caused by prevention of initial spheroid attachment: indeed, the ability of spheroids treated with anti-CD157 mAb to spread and disaggregate over the mesothelium is unaffected. Mesothelium damage typically occurring in the area surrounding the attached spheroids is largely prevented when CD157 is blocked. This suggests that CD157 expressed by juxtaposed tumor and mesothelial cells behaves as a gatekeeper governing an early step of OvCa invasion.

Finally, the contribution of the spheroids to tumor dissemination was assessed by monitoring disaggregation on the main components of the submesothelial basal membrane. Spheroids treated with anti-CD157 mAb are much less prone to disaggregate and disseminate on FN and LN. The result is that the area of disaggregation observed after 24 h treatment with anti-CD157 mAb is ~50% smaller than that of control spheroids. The effects mediated by CD157 are weak on type I collagen. A possible explanation is that the role of CD157 is masked by $\alpha_2\beta_1$ and $\alpha_3\beta_1$ Coll I receptors, which are reported as exerting a role in the regulation of OvCa spheroid dissemination on Coll I (44).

The proof-of-principle that CD157 is an important regulator of serous OvCa invasion and dissemination is provided by clinical data. First, the analysis of tissue samples from OvCa patients demonstrates that CD157 is expressed by the majority of tumors. Intratumoral CD157 expression is heterogeneous both in terms of levels and subcellular localization, a characteristic shared by many other molecules, reflecting the variability of the antigenic phenotype of solid

tumors. At present, it is unknown whether the heterogeneous expression and localization of CD157 may affect its function or its involvement in cancer biology.

Second, the results show that levels of CD157 expression at/above the median are significantly associated with rapid tumor relapse. Patients with tumor expressing CD157 at/above the median have a poorer prognosis than those characterized by CD157 expression below the median. Furthermore, iii) CD157 is a marker of poor prognosis in the serous subtype, the most frequent (~60% to 80%) and aggressive type of OvCa. Indeed, patients with serous ovarian cancer with CD157 H-score ≥60 are characterized by a much briefer DFS and OS than those with CD157 H-score <60. The multivariate survival analysis based on the Cox proportional model strengthened the prognostic value of the CD157 H-score by showing that CD157 is an independent prognostic factor of tumor relapse shortly after surgical debulking in ovarian cancer. Furthermore, in patients with serous carcinoma, CD157 H-score is a powerful independent predictive variable for disease recurrence and survival.

These observations are consistent with data derived from in vitro experiments and substantiate the conclusion that the presence of CD157 is paralleled by enhanced migratory and invasive properties of malignant cells. These facilitate peritoneal dissemination of the tumor and ultimately determine the clinical outcome. This is confirmed by the observation that forced expression of CD157 in $CD157^-$ NIH:OVCAR-3 line significantly increases motility, a prerequisite for dissemination. In contrast, CD157 blockage by specific mAb in vitro, or its weak expression in patients yield reduced invasion and migration of tumor cells.

The results obtained in patients indicate that CD157 marks tumor relapse in human epithelial serous OvCa. It therefore should be considered as a novel candidate molecule for use in conjunction with conventional diagnostic markers to help formulate dependable prognostic criteria in clinics. Further study is needed to define the molecular mechanisms through which CD157 operates.

New experimental approaches based on antibody-directed therapy and intraperitoneal injection have furnished promising new strategies for the treatment of OvCa dissemination (45,46). It is tempting to predict that CD157 may serve as a novel target for therapies in the control of invasion and dissemination of the peritoneal cavity by serous OvCa cells after surgical debulking.

Study limitations

The role of CD157 in the control of peritoneal dissemination and invasion of ovarian cancer was studied using in vitro models that may not thoroughly represent the situation in vivo. Results from in vivo animal models will allow more definitive conclusions to be drawn.

Funding

This work was supported by grants from the Italian Association for Cancer Research (AIRC, MFAG 6312 to E.O.); from the Italian Ministry for University and Scientific Research (PRIN 2006 and 60% Projects to A.F.); from Ricerca Sanitaria Finalizzata e Ricerca Scientifica Applicata (Regione Piemonte 2007-2008 to A.F.), and from International Foundation for Research in Experimental Medicine.

Notes

R.P. is supported by an AIRC fellowship and is a member of the Ph.D. program in "Human Genetics", P.B. is a member of the Ph.D. program in "Tumor Localization", N.LB. and G.N. of the Ph.D. program in "Complexity in Post-Genomic Biology", University of Turin, Turin Italy.

We thank A.L. Horenstein (University of Turin) for assistance with antibody purification, and are greatly indebted to Fabio Malavasi (University of Turin) for his advice and critical reading of the manuscript. The authors are grateful to Paola Berchialla (University of Turin) for her assistance with the statistical analysis.

Conflict of interest: The authors have no conflict of interest to declare.

References

1. Cannistra SA. Cancer of the ovary. *N Engl J Med.* 2004;351(24):2519-2529.
2. Kobel M, Kalloger SE, Boyd N, et al. Ovarian Carcinoma subtypes are different diseases: implications for biomarker studies. *PLoS Med.* 2008;5(12):e232.
3. Auersperg N, Wong AS, Choi KC, Kang SK, Leung PC. Ovarian surface epithelium: biology, endocrinology, and pathology. *Endocr Rev.* 2001;22(2):255-288.
4. Naora H, Montell DJ. Ovarian cancer metastasis: integrating insights from disparate model organisms. *Nat Rev Cancer* 2005;5(5):355-366.
5. Cannistra SA, Kansas GS, Niloff J, DeFranzo B, Kim Y, Ottensmeier C. Binding of ovarian cancer cells to peritoneal mesothelium in vitro is partly mediated by CD44H. *Cancer Res.* 1993;53(16):3830-3838.
6. Landen CN, Jr., Birrer MJ, Sood AK. Early events in the pathogenesis of epithelial ovarian cancer. *J Clin Oncol.* 2008;26(6):995-1005.
7. Tay SK, Rajesh H. Brain metastases from epithelial ovarian cancer. *Int J Gynecol Cancer* 2005;15(5):824-829.
8. Leroy-Dudal J, Demeilliers C, Gallet O, et al. Transmigration of human ovarian adenocarcinoma cells through endothelial extracellular matrix involves alphav integrins and the participation of MMP2. *Int J Cancer* 2005;114(4):531-543.
9. Rieppi M, Vergani V, Gatto C, et al. Mesothelial cells induce the motility of human ovarian carcinoma cells. *Int J Cancer* 1999;80(2):303-307.
10. Freedman RS, Deavers M, Liu J, Wang E. Peritoneal inflammation - A microenvironment for Epithelial Ovarian Cancer (EOC). *J Transl Med.* 2004;2(1):23.
11. Lessan K, Aguiar DJ, Oegema T, Siebenson L, Skubitz AP. CD44 and beta1 integrin mediate ovarian carcinoma cell adhesion to peritoneal mesothelial cells. *Am J Pathol.* 1999;154(5):1525-1537.

12. Salmi M, Jalkanen S. Cell-surface enzymes in control of leukocyte trafficking. *Nat Rev Immunol*. 2005;5(10):760-771.

13. Ferrero E, Malavasi F. Human CD38, a leukocyte receptor and ectoenzyme, is a member of a novel eukaryotic gene family of nicotinamide adenine dinucleotide+-converting enzymes: extensive structural homology with the genes for murine bone marrow stromal cell antigen 1 and aplysian ADP-ribosyl cyclase. *J Immunol.* 1997;159(8):3858-3865.

14. Malavasi F, Deaglio S, Funaro A, et al. Evolution and function of the ADP ribosyl cyclase/CD38 gene family in physiology and pathology. *Physiol Rev.*2008;88(3):841-886.

15. Kaisho T, Ishikawa J, Oritani K , et al. BST-1, a surface molecule of bone marrow stromal cell lines that facilitates pre-B-cell growth. *Proc Natl Acad Sci USA* 1994;91(12) 5325-5329.

16. Goldstein SC, Todd RF, 3rd. Structural and biosynthetic features of the Mo5 human myeloid differentiation antigen. *Tissue Antigens* 1993;41(4):214-218.

17. Ortolan E, Vacca P, Capobianco A, et al. CD157, the Janus of CD38 but with a unique personality. *Cell Biochem Funct.* 2002;20(4):309-322.

18. Ortolan E, Tibaldi EV, Ferranti B, et al. CD157 plays a pivotal role in neutrophil transendothelial migration. *Blood* 2006;108(13):4214-4222.

19. Ross JA, Ansell I, Hjelle JT, Anderson JD, Miller-Hjelle MA, Dobbie JW. Phenotypic mapping of human mesothelial cells. *Adv Perit Dial.* 1998;14:25-30.

20. Itoh M, Ishihara K, Hiroi T, et al. Deletion of bone marrow stromal cell antigen-1 (CD157) gene impaired systemic thymus independent-2 antigen-induced IgG3 and mucosal TD antigen-elicited IgA responses. *J Immunol.* 1998;161(8):3974-3983.

21. Ishihara K, Hirano T. BST-1/CD157 regulates the humoral immune responses in vivo. *Chem Immunol.* 2000;75:235-255.

22. Funaro A, Ortolan E, Bovino P, et al. Ectoenzymes and innate immunity: the role of human CD157 in leukocyte trafficking. *Front Biosci.* 2009;14:929-943.

23. Liang F, Qi RZ, Chang CF. Signalling of GPI-anchored CD157 via focal adhesion kinase in MCA102 fibroblasts. *FEBS Lett.* 2001;506(3):207-210.

24. Lavagno L, Ferrero E, Ortolan E, Malavasi F, Funaro A. CD157 is part of a supramolecular complex with CD11b/CD18 on the human neutrophil cell surface. *J Biol Regul Homeost Agents* 2007;21(1-2):5-11.

25. Funaro A, Ortolan E, Ferranti B, et al. CD157 is an important mediator of neutrophil adhesion and migration. *Blood* 2004;104(13):4269-4278.

26. Horenstein AL, Sizzano F, Lusso R, et al. CD38 and CD157 ectoenzymes mark cell subsets in the human corneal limbus. *Mol Med.* 2009;15(3-4):76-84.

27. Kelm JM, Timmins NE, Brown CJ, Fussenegger M, Nielsen LK. Method for generation of homogeneous multicellular tumor spheroids applicable to a wide variety of cell types. *Biotechnol Bioeng.* 2003;83(2):173-180.

28. Burleson KM, Boente MP, Pambuccian SE, Skubitz AP. Disaggregation and invasion of ovarian carcinoma ascites spheroids. *J Transl Med.* 2006;4:6.

29. Burleson KM, Hansen LK, Skubitz AP. Ovarian carcinoma spheroids disaggregate on type I collagen and invade live human mesothelial cell monolayers. *Clin Exp Metastasis* 2004;21(8):685-697.

30. Kerfoot C, Huang W, Rotenberg SA. Immunohistochemical analysis of advanced human breast carcinomas reveals downregulation of protein kinase C alpha. *J Histochem Cytochem.* 2004;52(3):419-422.

31. Hood JD, Cheresh DA. Role of integrins in cell invasion and migration. *Nat Rev Cancer* 2002;2(2):91-100.

32. Sawada K, Mitra AK, Radjabi AR, et al. Loss of E-cadherin promotes ovarian cancer metastasis via alpha 5-integrin, which is a therapeutic target. *Cancer Res.* 2008;68(7):2329-2339.

33. Witz CA, Montoya-Rodriguez IA, Cho S, Centonze VE, Bonewald LF, Schenken RS. Composition of the extracellular matrix of the peritoneum. *J Soc Gynecol Investig.* 2001;8(5):299-304.

34. Zietarska M, Maugard CM, Filali-Mouhim A, Alam-Fahmy M, Tonin PN, Provencher DM, et al. Molecular description of a 3D in vitro model for the study of epithelial ovarian cancer (EOC). *Mol Carcinog.* 2007;46(10):872-885.

35. Shield K, Riley C, Quinn MA, Rice GE, Ackland ML, Ahmed N. Alpha2beta1 integrin affects metastatic potential of ovarian carcinoma spheroids by supporting disaggregation and proteolysis. *J Carcinog.* 2007;6:11.

36. Le Page C, Ouellet V, Madore J, Ren F, Hudson TJ, Tonin PN, et al. Gene expression profiling of primary cultures of ovarian epithelial cells identifies novel molecular classifiers of ovarian cancer. *Br J Cancer* 2006;94(3):436-445.

37. Shield K, Ackland ML, Ahmed N, Rice GE. Multicellular spheroids in ovarian cancer metastases: Biology and pathology. *Gynecol Oncol.* 2009;113(1):143-148.

38. Rainaldi G, Calcabrini A, Arancia G, Santini MT. Differential expression of adhesion molecules (CD44, ICAM-1 and LFA-3) in cancer cells grown in monolayer or as multicellular spheroids. *Anticancer Res.* 1999;19(3A):1769-1778.

39. Casey RC, Burleson KM, Skubitz KM, et al. Beta 1-integrins regulate the formation and adhesion of ovarian carcinoma multicellular spheroids. *Am J Pathol.* 2001;159(6):2071-2080.

40. Guo W, Giancotti FG. Integrin signalling during tumour progression. *Nat Rev Mol Cell Biol.* 2004;5(10):816-826.

41. Miranti CK, Brugge JS. Sensing the environment: a historical perspective on integrin signal transduction. *Nat Cell Biol.* 2002;4(4):E83-90.

42. Sawada M, Shii J, Akedo H, Tanizawa O. An experimental model for ovarian tumor invasion of cultured mesothelial cell monolayer. *Lab Invest.* 1994;70(3):333-338.

43. Yamada KM, Cukierman E. Modeling tissue morphogenesis and cancer in 3D. *Cell* 2007;130(4):601-610.

44. Ellerbroek SM, Wu YI, Overall CM, Stack MS. Functional interplay between type I collagen and cell surface matrix metalloproteinase activity. *J Biol Chem.* 2001;276(27):24833-24842.

45. Yap TA, Carden CP, Kaye SB. Beyond chemotherapy: targeted therapies in ovarian cancer. *Nat Rev Cancer* 2009;9(3):167-181.

46. Collinson F, Jayson G. New therapeutic agents in ovarian cancer. *Curr Opin Obstet Gynecol*. 2009;21(1):44-53.

Figure legends

Figure 1. Expression of CD157 in primary cultures of OvCa cells and OvCa lines at surface protein and mRNA levels. Flow cytometric analysis of the surface expression of CD157 in primary OvCa cells (**A**) and OvCa lines (**C**) compared with isotype staining (shaded). Total RNA was extracted from primary OvCa cells **(B)** and tumor lines **(D)**, reverse transcribed, and amplified by RT-PCR. MONOMAC-6 and K562 lines served as the positive and negative controls, respectively. **E**) Western blot analysis of CD157 immunoprecipitated from 4 CD157-positive OvCa lines and MONOMAC-6 line. **F**) Cobblestone-like appearance of a confluent peritoneal mesothelial cell (HPMC) monolayer obtained from peritoneal washing. **G**) Representative flow histogram of CD157 expression in HPMC compared with isotype staining (shaded). **H**) Expression of CD157 on confluent HPMC analyzed by laser-scanning confocal microscopy (left panel) or by Nomarski optics (DIC) (right panel) (scale bar = 20 μm)

Figure 2. Expression of CD157 in OvCa cells from primary tumor and ascites. **A**) Flow cytometric analysis shows CD157 staining on almost all of the OvCa 622 cells derived from primary tumor fragments (left panel, black line) but only on a limited number of cells from ascites (right panel, black line). CD157 expression is increased in cells from ascites after 2 days in culture (right panel, green line). **B**) Expression of CD157 (fold change of mean fluorescence intensity, MFI) was evaluated in OvCa 2947 spheroids in suspension after 12 h (blue line) and 24 h (green line) in culture. **C**) Confocal microscopy analysis of spheroids from OvCa 2947 shows that CD157 is expressed exclusively on the cells forming the outer layer of the spheroid (left panel). As the spheroid disaggregates, the released isolated cells reacquire CD157 expression (middle panel). The monolayer obtained after 3 days in culture presents homogeneous expression of CD157 (right panel). Cells were viewed by FITC channel (top panels) and Nomarski optics (DIC, bottom panels) (scale bar = 100 μm).

Figure 3. Effects of CD157 ligation on tumor cell invasion through and adhesion to ECM proteins. Tumor cells were treated (20 min) with the indicated mAb (10 μg/ml), added (**A**) to

matrigel or (**B**) to uncoated or fibronectin (FN), laminin (LN) and collagen I (Coll I)-coated filters and incubated for 16 h. Invasion across matrigel is expressed as number of cells/mm^2 of the transwell filters. Invasion across FN, LN and Coll I is expressed as percentage of migrated cells compared to migrated cells in the control filters. Results represent the mean values (n = 3) and 95% confidence intervals (CI) (error bars). **C**) OvCa 2947, SKOV-3 and OV-90 cells were treated (20 min) with the indicated mAb (10 μg/ml) and plated onto 96 well plates uncoated or coated with FN, LN and Coll I for 1 h, then washed, fixed, stained with crystal violet and counted. Results represent the mean values of 3 experiments performed in quadruplicate and 95% CI. *P* values (two sided) listed were derived from ANOVA with Bonferroni correction by comparing cells treated with anti-CD157 (grey bars) or anti-β1-integrin (black bars) mAb with cells treated with mIgG (white bars).

Figure 4. Effect of exogenous expression of CD157 on tumor cell migration. **A**) Flow cytometric analysis of NIH:OVCAR-3 cells transfected with the pcDNA3.1 vector containing either full-length *CD157* cDNA or no insert (mock), shows surface expression of CD157 in NIH:OVCAR-3-3D11 (left panel) and NIH:OVCAR-3-2G5 (middle panel) clones, but not in mock-transfected NIH:OVCAR-3 cells (right panel). **B**) NIH:OVCAR-3-3D11 (left panels), NIH:OVCAR-3-2G5 (middle panel) and NIH:OVCAR-3-mock (right panels) were grown as monolayers, wounded and photographed at time 0 and after 24 h incubation at 37 °C (scale bar = 200 μm). **C**) Quantitative results of the percentage of wound healing (calculated by measuring 20 randomly chosen distances across the wound at time 0 and 24 h, divided by the distance measured at time 0) indicate that the migratory capacity of NIH:OVCAR-3-3D11 and NIH:OVCAR-3-2G5 cells is approximately twice that of NIH:OVCAR-3-mock cells. Results represent the means of three experiments and 95% confidence intervals. *P* values (two sided) were derived from ANOVA with Bonferroni correction by comparing NIH:OVCAR-3-3D11 or -2G3 (grey bars) with mock cells (white bar).

Figure 5. Role of CD157 in the controls of spheroid dissemination and invasion. **A**) OV-90 spheroids were seeded on live peritoneal mesothelial cells (HPMC) monolayers in the presence of the indicated mAb (10 μg/ml) and the area was measured at days 0, 1, 3 and 7. Spheroid dissemination was defined as spheroid disaggregation and spreading over the HPMC monolayer. Results represent the fold increase in area of 80-100 spheroids/condition (n = 2). Box and whisker plots show the fold increase in area of spheroids treated with mIgG (white boxes), anti-CD157 (grey boxes) and anti-β1 integrin (black boxes) mAb. The box ranges from the 25th to the 75th percentile (interquartile range) and whisker extend to the highest and lowest observed values. The median is indicated by the horizontal line across the box. *P* values (two sided) listed were derived from Kruskal-Wallis nonparametric test with the Dunn's correction by comparing spheroids treated with anti-CD157 or anti-β1-integrin mAb with spheroids treated with mIgG. **B**) Digital photographs of spheroids plated on HPMC in the presence of anti-CD157 (top panels) or mIgG (bottom panels). Arrows delineate the perimeter of disseminating (anti-CD157-treated) or invading (mIgG-treated) spheroids (scale bar = 200 μm). **C**) The number of spheroids generating foci of invasion was counted at days 1, 3 and 7 for each condition. Results represent the percentage of mIgG (white bars), anti-CD157 (grey bars) or anti-β1 integrin (black bars)-treated spheroids that invaded the HPMC monolayer. *P* value (two sided) was obtained using the Chi-square test. **D**) CD157 is not involved in the adhesion of OvCa cells to HPMC. Confluent HPMC and OvCa cells were treated with the indicated mAb, then OvCa cells were seeded on HPMC and allowed to adhere (1 h at 37 °C). Non adherent OvCa cells were washed off before MTT staining. Results represent the mean values and 95% confidence intervals (CI) of 3 experiments performed in quadruplicate and are expressed as percentage of adhesion of the mIgG-treated control. *P* values (two sided) listed were derived from ANOVA with Bonferroni correction by comparing cells treated with anti-CD157 (grey bars) or anti-β1-integrin (black bars) mAb with cells treated with mIgG (white bars).

E) Spheroids were allowed to adhere to fibronectin (FN)-coated wells for 30 min before the addition of anti-CD157, anti-β1 integrin mAb or mIgG. Spheroids were photographed at time 0 and at 24 h and the increase of disaggregation area is reported. Results represent the means and 95% CI of the fold change in area of 50-90 spheroids/condition (n = 3). *P* values (two sided) listed were derived from ANOVA with Bonferroni correction by comparing cells treated with anti-CD157 (grey bars) or anti-β1 integrin (black bars) mAb with cells treated with mIgG (white bars). **F**) Digital photographs showing the morphology of a typical spheroid seeded on FN at day 0 and day 1 in the presence of anti-CD157 mAb (left panels) or mIgG (right panels). Few isolated cells are visible in the area surrounding the spheroid after CD157 exposure (scale bar = 200 μm).

Figure 6. Immunohistochemical localization and definition of the expression levels (H-score) of CD157 in epithelial OvCa samples. Tissue sections from formalin-fixed, paraffin-embedded epithelial OvCa were stained with anti-CD157 mAb (brown staining, hematoxylin counterstaining). **A**) Endometrioid carcinoma showing cytoplasmic localization of CD157 (original magnification, x400). **B**) Serous papillary carcinoma showing dot-like cytoplasmic and membrane CD157 staining with apical localization (original magnification, x200). **C**) Serous papillary carcinoma showing dot-like cytoplasmic CD157 staining with apical localization (original magnification, x200). **D**) Normal epithelial cells showing a granular cytoplasmic CD157 staining mainly localized at the basolateral surface (original magnification, x100) (scale bars = 50 μm). **E**) The examined cohort was categorized by histotype and plotted against the CD157 expression level (defined as H-score). The median H-score (60) was used as the cut-off criterion. Each data point corresponds to the CD157 H-score in individual tumor samples and the horizontal lines represent the mean of values.

Figure 7. CD157 expression and clinical outcome. Kaplan Meier analysis of disease-free (DFS) (**A**) and overall survival (OS) (**B**) in 88 patients according to CD157 expression levels at/above (H score ≥60) or below (H score <60) the median. Median DFS in patients with CD157 H-score ≥60 and H score <60 was 30 months (95% confidence interval (CI) = 20.99 to 39.00) and not

reached, respectively (log-rank test, P = .004). **B**) The association between CD157 expression level and OS did not reach statistical significance (log-rank test, P = .059). In serous carcinoma, median DFS (**C**) in patients with CD157 H-score ≥60 and H-score <60 was 18 months (95% CI = 5.92 to 30.07) and not reached, respectively (log-rank test, P = .005). The median OS (**D**) in patients with CD157 H-score ≥60 and H-score <60 was 45 months (95% CI = 21.21 to 68.79) and not reached, respectively (log-rank test, P = .024). In non-serous carcinomas (**E-F**) CD157 H-score association between and DFS and OS was not significant. P values were determined using the log-rank test.

Primary epithelial OvCa	Source	Histopathology of the original tumor
OvCa 622	ascites/primary tumor	cystoadenocarcinoma, poorly differentiated, papillary serous, (pT3bG3)
OvCa 860	primary tumor	mucinous cystic tumor, borderline, (pT1aG1)
OvCa 1349	primary tumor	adenocarcinoma, poorly differentiated, papillary serous, (pT3bG3)
OvCa 1554	primary tumor	cystoadenocarcinoma, papillary serous, (pT3bG3)
OvCa 1996	primary tumor	cystoadenocarcinoma, poorly differentiated, endometrioid, (pT1aG2)
OvCa 2947	primary tumor	cystoadenocarcinoma, poorly differentiated, papillary serous, (pT3cG3)

Table 1. Histopathology of fresh primary epithelial tumors

	number of cases	H-score ≥ 60	H-score <60	*P*
Ovarian carcinomas (n, %)	88	50 (57%)	38 (43%)	
Age at surgery (years)				**0.292***
mean ± SD	58.3±11.6	59.5±11.5	56.8±11.6	
median (range)	58 (29-83)	59 (33-82)	57 (29-83)	
Histological type				**0.569**
Serous papillary	51	30	21	
Endometriod	12	7	5	
Mucinous	4	1	3	
Clear cells	9	7	2	
Undifferentiated	12	5	7	
Histological grade				**0.489**
Low (G1-G2)	28	14	14	
High (G3)	60	36	24	
Disease stage				**0.074**
Low (I-II)	30	13	17	
High (III-IV)	58	37	21	
Follow-up				
NED[†]	35	13	22	
DOC[‡]	4	2	2	
AWD[§]	12	10	2	
DOD[¶]	37	25	12	

Table 2. Clinical and pathological characteristics of epithelial ovarian cancer patients and their association to CD157 expression, as assessed by immunohistochemistry.

*determined with Mann-Whitney test; [†]NED = no evidence of disease; [‡]DOC = died from other causes; [§]AWD = alive with disease, [¶]DOD = died of disease.
P values are determined using Chi-square or Fisher's exact test.

A

		Univariate analysis			Multivariate analysis		
Factors		**HR***	**95% CI†**	***P***	**HR**	**95% CI**	***P***
CD157 H-score (<60 vs. ≥60)	all histotypes	2.344	1.281-4.287	0.006	2.438	1.247-4.764	0.009
	serous	2.725	1.309-5.673	0.007	3.008	1.351-6.694	0.007
Histological type (non serous *vs* serous)		2.200	1.202-4.025	0.011	2.139	1.128-4.055	0.020
Disease stage (I-II *vs.* III-IV)	all histotypes	4.843	2.176-10.778	< .001	3.489	1.531-7.949	0.003
	serous	3.626	1.401-9.388	0.008	2.928	1.126-7.614	0.028
Histological grade (G1-G2 *vs.* G3)	all histotypes	1.569	0.835-2.948	0.161	1.092	0.562-2.120	0.795
	serous	1.016	0.489-2.111	0.966	0.847	0.405-1.771	0.658
Age at surgery (<58 *vs.* ≥58)	all histotypes	0.948	0.546-1.646	0.850	1.087	0.610-1.937	0.778
	serous	0.839	0.435-1.616	0.600	1.016	0.508-2.029	0.965
CD157 localization cytoplasmic *vs.* membranous	all histotypes	1.249	0.671-2.326	0.483	1.314	0.692-2.495	0.403
	serous	1.199	0.586-2.453	0.618	1.463	0.698-3.066	0.314

B

		Univariate analysis			Multivariate analysis		
Factors		**HR***	**95% CI†**	***P***	**HR**	**95% CI**	***P***
CD157 H-score (<60 *vs.* ≥60)	all histotypes	1.918	0.962-3.826	0.064	2.110	0.966-4.607	0.061
	serous	2.619	1.097-6.250	0.030	3.443	1.273-9.308	0.015
Histological type (non serous *vs.* serous)		1.807	0.892-3.661	0.100	1.670	0.780-3.575	0.187
Disease stage (I-II *vs.* III-IV)	all histotypes	7.581	2.327-24.699	0.001	6.341	1.893-21.236	0.003
	serous	12.844	1.737-94.953	0.012	10.62	1.428-78.987	0.021
Histological grade (G1-G2 *vs.* G3)	all histotypes	1.165	0.575-2.361	0.671	0.857	0.399-1.838	0.691
	serous	0.862	0.374-1.988	0.727	0.907	0.375-2.198	0.830
Age at surgery (<58 *vs.* ≥58)	all histotypes	1.276	0.665-2.450	0.463	1.623	0.796-3.311	0.183
	serous	1.436	0.659-3.131	0.363	2.072	0.876-4.903	0.097
CD157 localization cytoplasmic *vs.* membranous	all histotypes	0.972	0.476-1.986	0.937	0.954	0.451-2.017	0.902
	serous	0.907	0.390-2.110	0.821	1.062	0.435-2.594	0.894

Table 3. Prognostic factors in the Cox proportional hazard model for disease-free (**A**) and overall (**B**) survival of patients with ovarian cancer.
*HR = hazard ratio
†CI = confidence interval

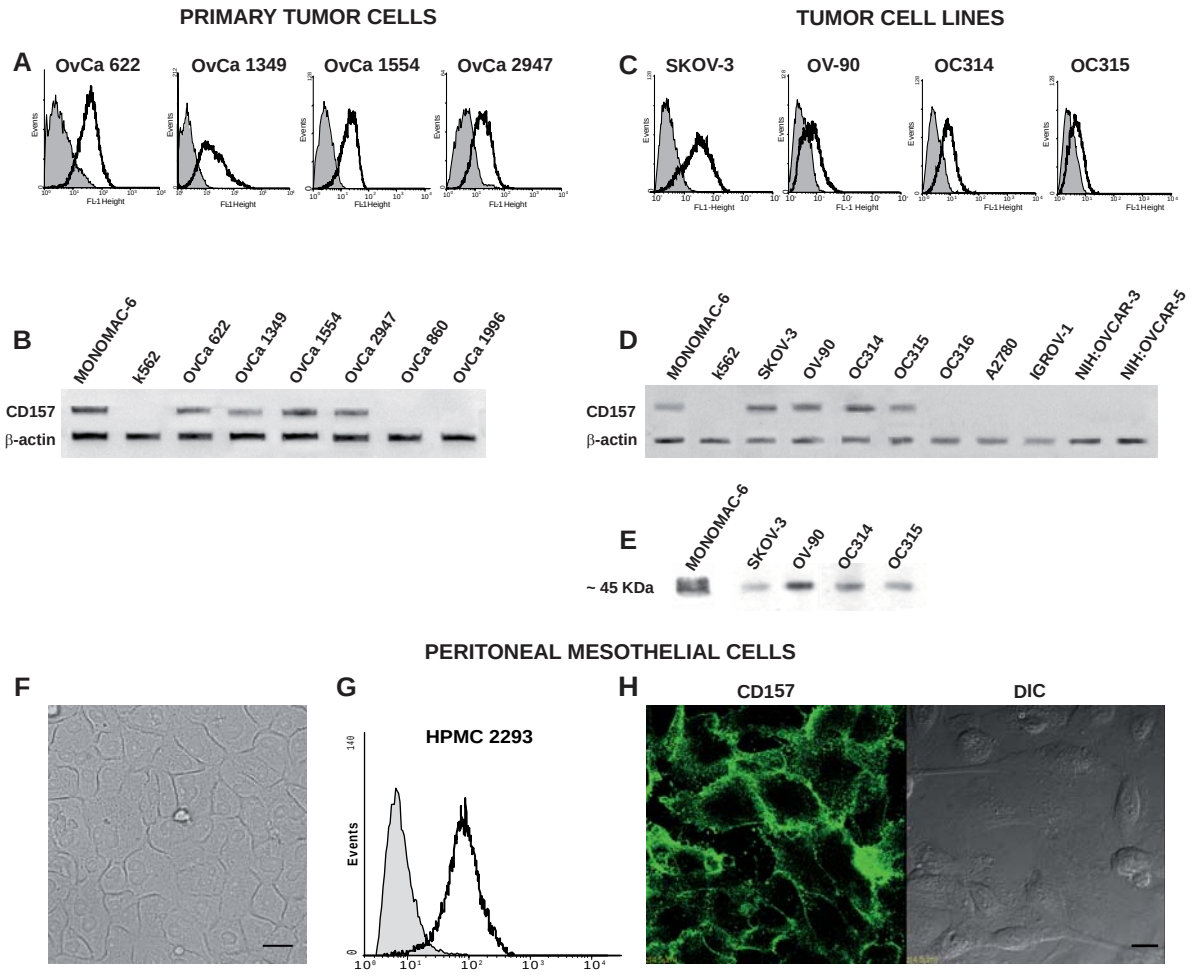
PRIMARY TUMOR CELLS
TUMOR CELL LINES
A
OvCa 622
OvCa 1349
OvCa 1554
OvCa 2947
C
SKOV-3
OV-90
OC314
OC315
B
MONOMAC-6
k562
OvCa 622
OvCa 1349
OvCa 1554
OvCa 2947
OvCa 860
OvCa 1996
CD157
β-actin
D
MONOMAC-6
k562
SKOV-3
OV-90
OC314
OC315
OC316
A2780
IGROV-1
NIH:OVCAR-3
NIH:OVCAR-5
CD157
β-actin
E
MONOMAC-6
SKOV-3
OV-90
OC314
OC315
~ 45 KDa
PERITONEAL MESOTHELIAL CELLS
F
G
HPMC 2293
Events
H
CD157
DIC

Figure 1

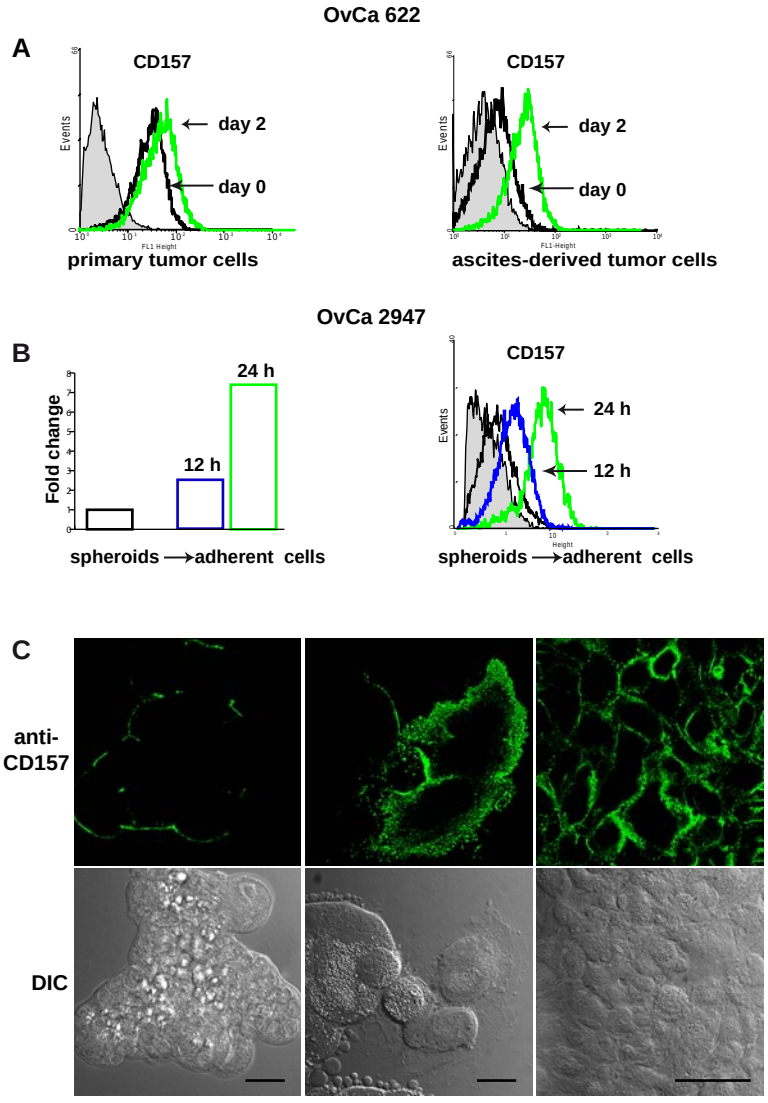
OvCa 622
A
CD157
day 2
day 0
Events
primary tumor cells
CD157
day 2
day 0
Events
ascites-derived tumor cells
OvCa 2947
B
24 h
12 h
Fold change
spheroids → adherent cells
CD157
24 h
12 h
Events
spheroids → adherent cells
C
anti-CD157
DIC

Figure 2

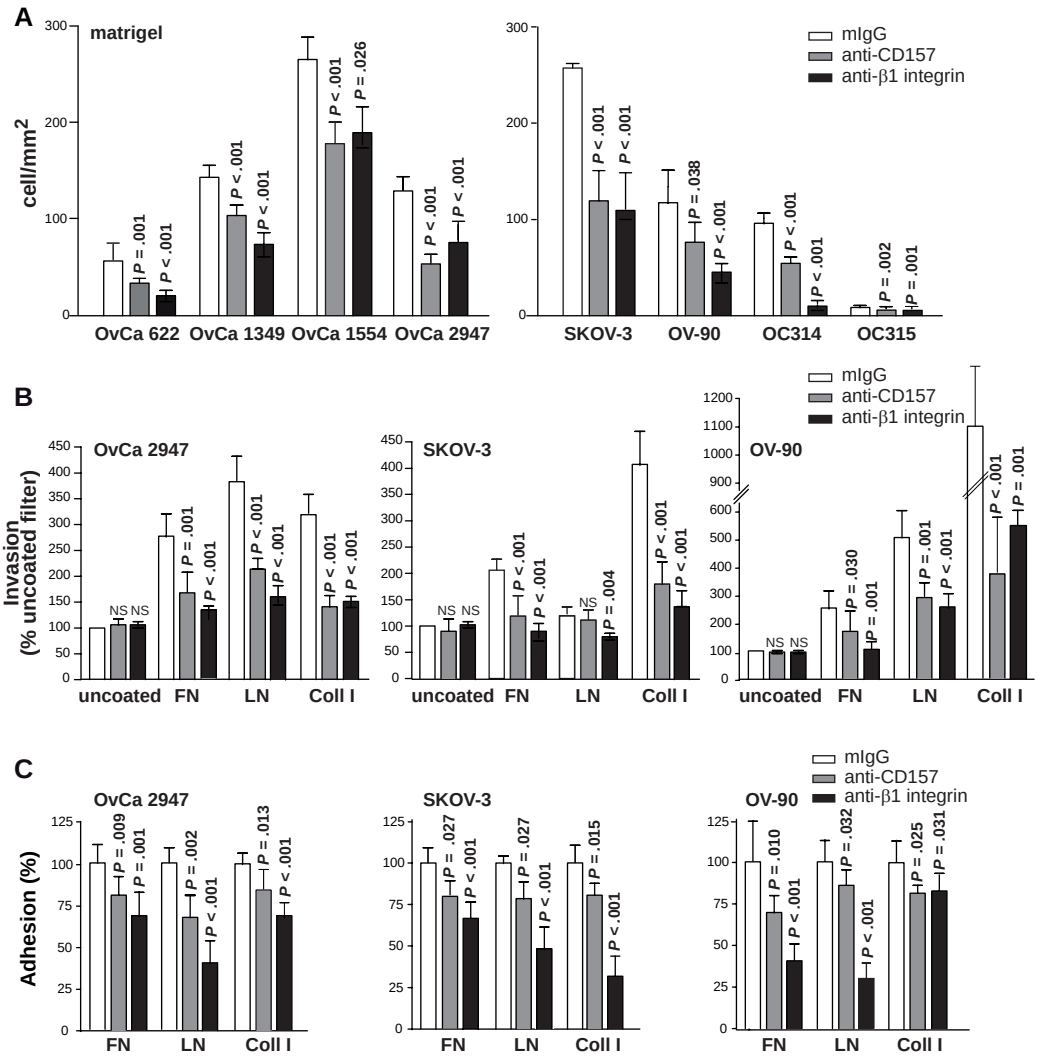
A
matrigel
cell/mm2
mIgG
anti-CD157
anti-β1 integrin
OvCa 622
OvCa 1349
OvCa 1554
OvCa 2947
SKOV-3
OV-90
OC314
OC315
B
Invasion
(% uncoated filter)
OvCa 2947
SKOV-3
OV-90
uncoated
FN
LN
Coll I
NS
C
Adhesion (%)
OvCa 2947
SKOV-3
OV-90
FN
LN
Coll I

Figure 3

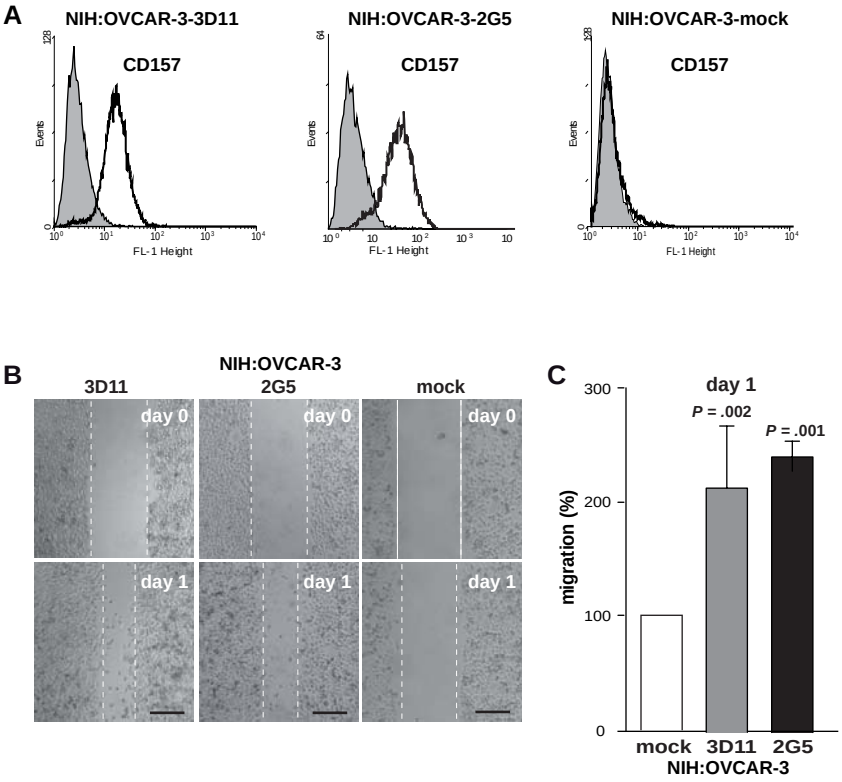
A
NIH:OVCAR-3-3D11
CD157
NIH:OVCAR-3-2G5
CD157
NIH:OVCAR-3-mock
CD157
Events
FL-1 Height
B
NIH:OVCAR-3
3D11
2G5
mock
day 0
day 1
C
day 1
P = .002
P = .001
migration (%)
300
200
100
0
mock
3D11
2G5
NIH:OVCAR-3

Figure 4

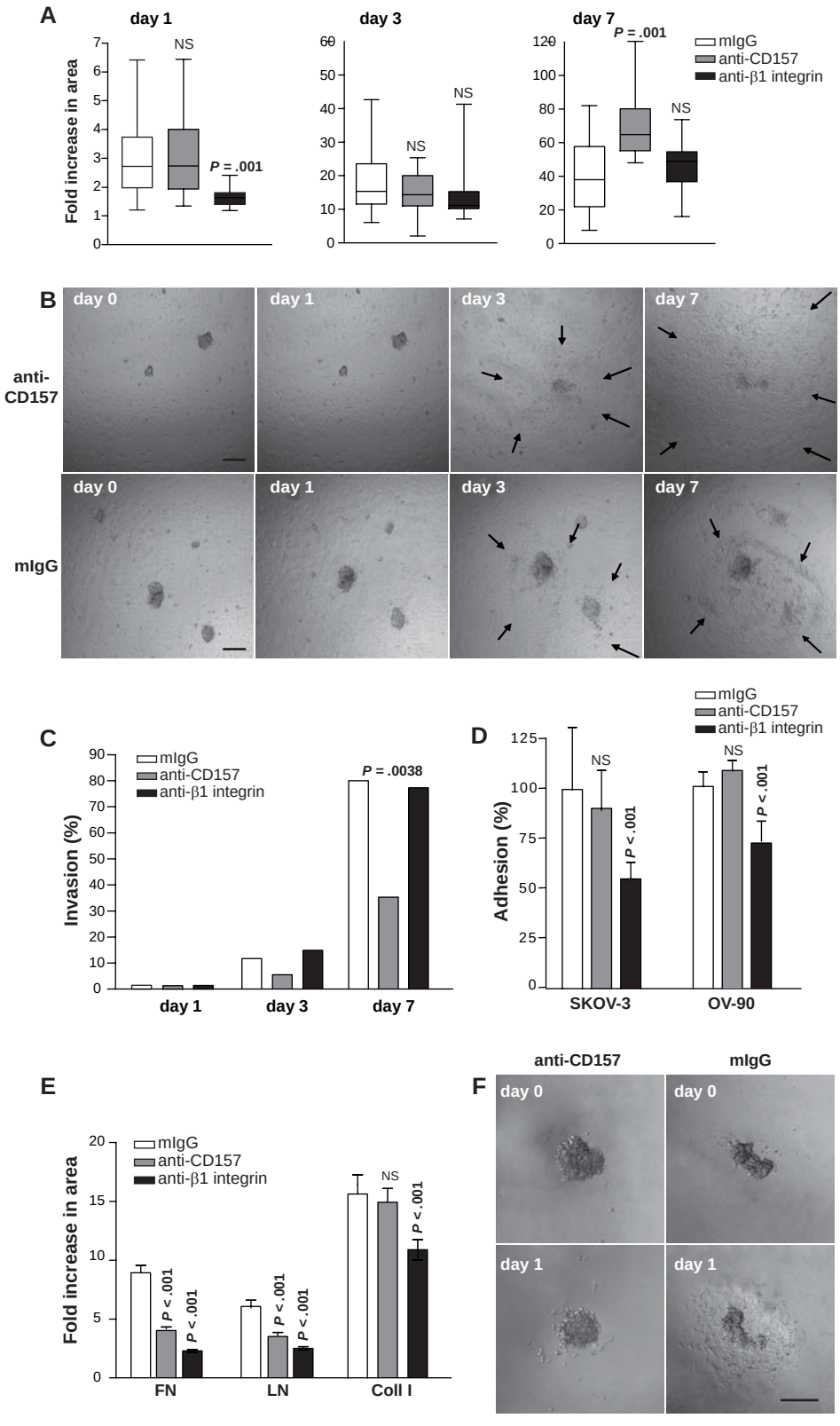
A
day 1
day 3
day 7
Fold increase in area
NS
P = .001
mIgG
anti-CD157
anti-β1 integrin
B
day 0
day 1
day 3
day 7
anti-CD157
mIgG
C
Invasion (%)
P = .0038
day 1
day 3
day 7
D
Adhesion (%)
P < .001
SKOV-3
OV-90
E
Fold increase in area
FN
LN
Coll I
F
anti-CD157
mIgG

Figure 5

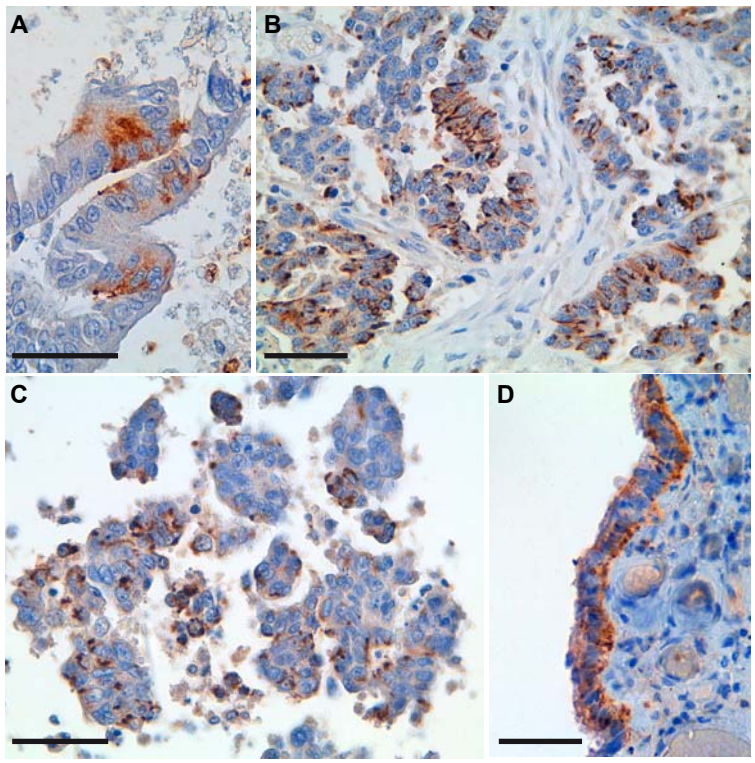
A
B
C
D

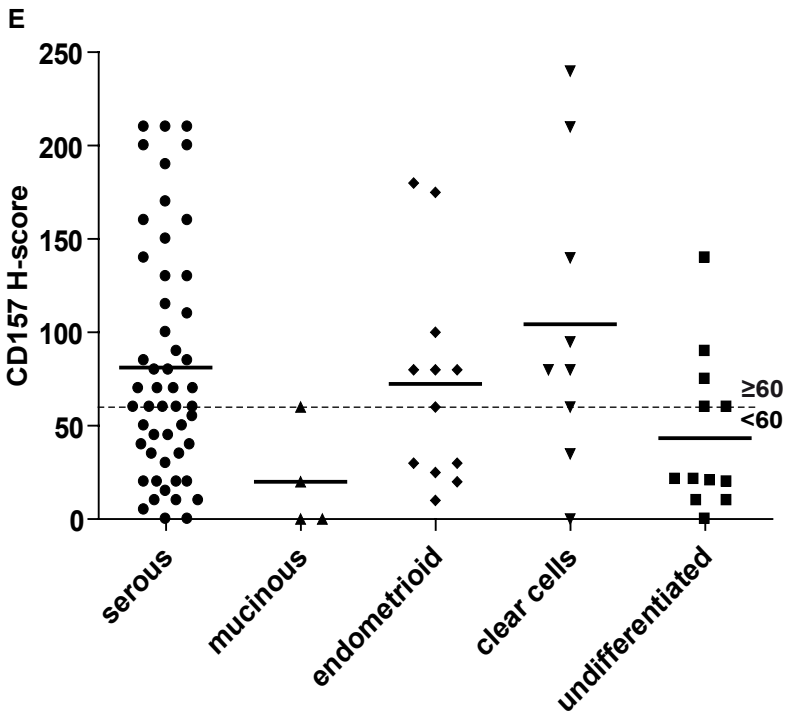
E
CD157 H-score
250
200
150
100
50
0
≥60
<60
serous
mucinous
endometrioid
clear cells
undifferentiated

Figure 6

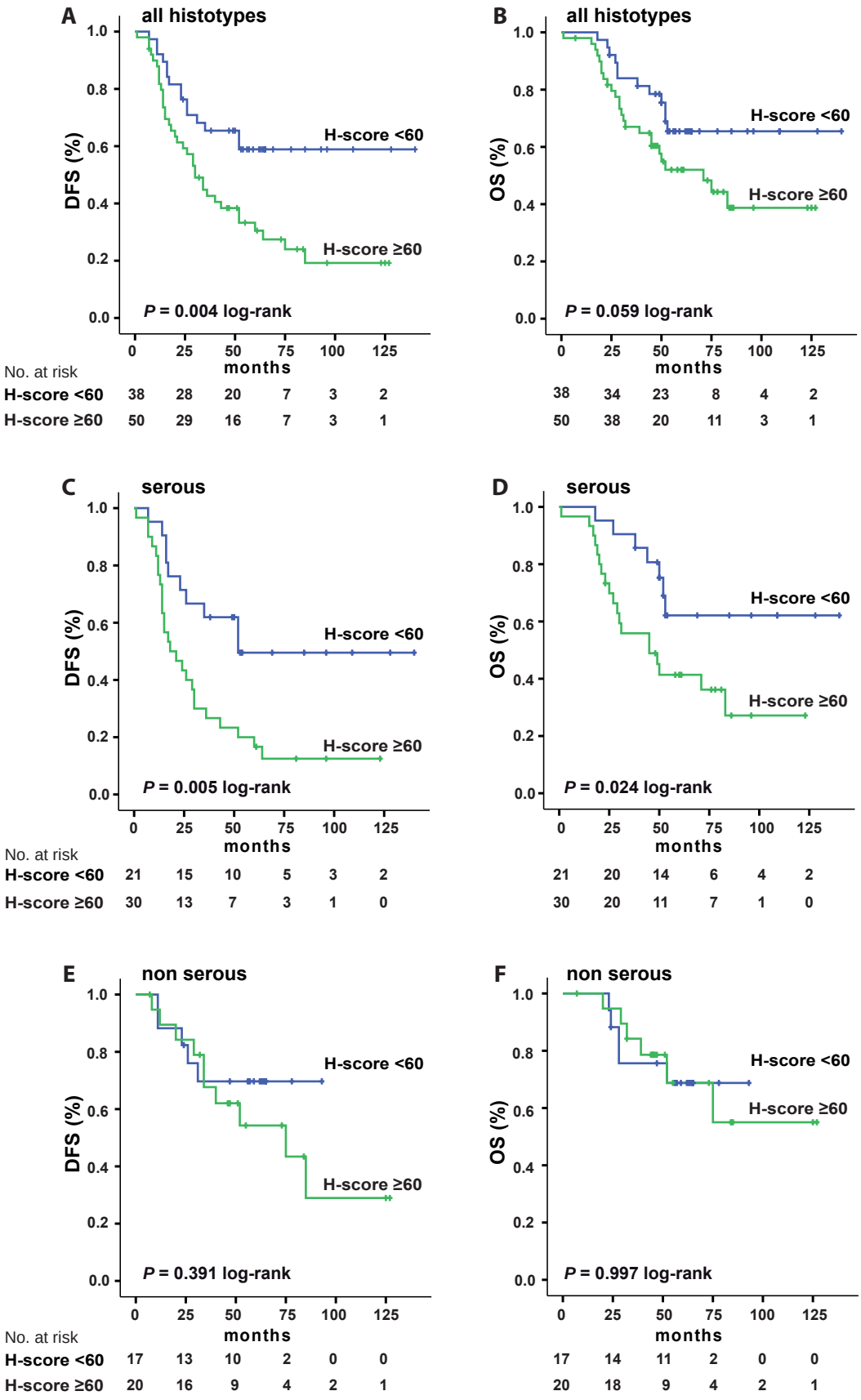
A
all histotypes
DFS (%)
1.0
0.8
0.6
0.4
0.2
0.0
H-score <60
H-score ≥60
P = 0.004 log-rank
0 25 50 75 100 125
months
No. at risk
H-score <60 38 28 20 7 3 2
H-score ≥60 50 29 16 7 3 1
B
all histotypes
OS (%)
H-score <60
H-score ≥60
P = 0.059 log-rank
0 25 50 75 100 125
months
38 34 23 8 4 2
50 38 20 11 3 1
C
serous
DFS (%)
H-score <60
H-score ≥60
P = 0.005 log-rank
0 25 50 75 100 125
months
No. at risk
H-score <60 21 15 10 5 3 2
H-score ≥60 30 13 7 3 1 0
D
serous
OS (%)
H-score <60
H-score ≥60
P = 0.024 log-rank
0 25 50 75 100 125
months
21 20 14 6 4 2
30 20 11 7 1 0
E
non serous
DFS (%)
H-score <60
H-score ≥60
P = 0.391 log-rank
0 25 50 75 100 125
months
No. at risk
H-score <60 17 13 10 2 0 0
H-score ≥60 20 16 9 4 2 1
F
non serous
OS (%)
H-score <60
H-score ≥60
P = 0.997 log-rank
0 25 50 75 100 125
months
17 14 11 2 0 0
20 18 9 4 2 1

Figure 7

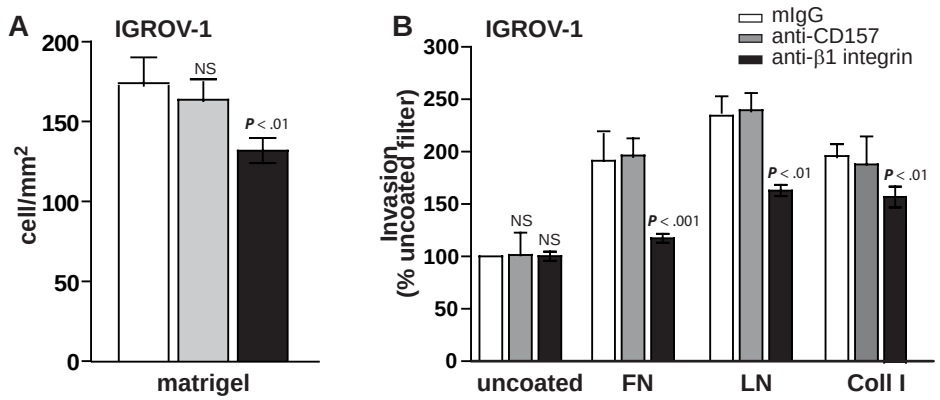

Effects of anti-CD157 mAb on CD157-negative tumor cell invasion through ECM proteins. IGROV-1 cells were treated (20 min) with the indicated mAb (10 μg/ml), added (**A**) to matrigel or (**B**) to uncoated or FN, LN and Coll I-coated filters and incubated for 16 h. Invasion across matrigel is expressed as number of cells/mm^2 of the transwell filters. Invasion across FN, LN and Coll I is expressed as percentage of migrated cells compared to migrated cells in the control filters (uncoated). Results represent the mean with 95% CI (error bars) (n = 3). *P* values (two sided) are referred to the comparison between cells treated with anti-CD157 or anti-β1-integrin mAb versus mIgG, and were derived from ANOVA with Bonferroni correction.

Supplementary Figure 1